Chaotic mixing in microfluidic devices driven by oscillatory cross flow

Frederick R. Phelan, Jr.,[a)] Nicholas R. Hughes, and Jai A. Pathak[b)]
Polymers Division, National Institute of Standards and Technology, Gaithersburg, Maryland 20899, USA

The kinematics of oscillatory cross flow has been studied numerically as a means for generating chaotic mixing in microfluidic devices for both confined and continuous throughput flow configurations. The flow is analyzed using numerical simulation of the unsteady Navier–Stokes equations combined with tracking of single and multispecies passive tracer particles. Two characteristics of chaotic flow are demonstrated: the stretching and folding of material lines leading to particle dispersion and a positive "effective" Lyapunov exponent. The primary mechanism for the generation of chaotic flow is a periodic combination of stretching (which occurs via shear in the channels) and rotation (which occurs via the timing of the oscillations), making these systems effective tendril-whorl type flows. First, the case of confined mixing is studied. It is shown that chaotic flow is generated in a cross-cell device when sinusoidally driven, out-of-phase, perpendicular fluid streams intersect in the flow domain. Calculations indicate that the flow becomes chaotic in the center region starting at a Strouhal number on the order of 1. A degree of mixing based on a relative mixing entropy as high as 91% is obtained. Approximately 10–15 sinusoidal cycles are needed in order to effectively mix different groups of passive tracer particles. In the second phase of the analysis, the cross flow mixing mechanism is utilized in a continuous operation by combining a throughput channel flow with an oscillatory cross flow in a configuration called the star-cell geometry. It is shown that the oscillatory flow remains chaotic even in combination with the throughput flow, and a degree of mixing in the 80%–90% range is obtained for the range of parameters studied here. [DOI: 10.1063/1.2830550]

INTRODUCTION

Mixing is an important issue in many chemical and biological applications using microfluidic devices[1] for a variety of reasons, including initiation of chemical reaction, chemical treatment of biological species, emulsification of immiscible components, and dispersion of gas phase bubbles or solid particles in liquid streams. While mixing is most naturally achieved through turbulent flow, microfluidic flows are normally low Reynolds number (Re) due to the very small length scales at which these devices are fabricated. This makes turbulent flow virtually impossible to achieve, and the mixing of fluids is generally "slow" and diffusion-controlled. The problem is further compounded by the fact that the Peclet number (Pe) for diffusion is usually rather large ($10 < Pe < 10^5$) in these systems,[1,2] making the required length scale for mixing in the streamwise (or throughput) direction unduly large.

Mixing can be greatly enhanced in laminar flow by subjecting the fluid to chaotic flow kinematics. The theory of chaotic mixing has been well developed due to the pioneering work of Ottino and co-workers, e.g., Refs. 3–17, as well as Aref and co-workers, e.g., Refs. 18–23. Recent works highlight the application of these principles to micromixing.[2,11,23] In chaotic advection, a term coined by Aref,[22] material lines undergo complex patterns of stretching and folding characterized mathematically as a horseshoe map.[3,5–7,9] Practically speaking, chaotic kinematics have a twofold effect on the mixing process. Nearby particle trajectories separate at an exponential rate described by a positive Lyapunov exponent,[24]

$$\lambda = \lim_{\substack{t \to \infty \\ \Delta x(0) \to 0}} \frac{1}{t} \ln \frac{|\Delta x(t)|}{|\Delta x(0)|}, \tag{1}$$

where $\Delta x(0)$ and $\Delta x(t)$ represent the separation of two particles at times 0 and t, respectively. Thus, as viewed from the Lagrangian sense, chaotic flow fields tend to lead to fluid particles becoming homogeneously dispersed via a mechanism due only to kinematics. The positive exponent also plays a role as viewed from the standpoint of the stretching of material lines and surfaces.[3,6] For two-dimensional (2D) flows, the stretching of a material element in a chaotic flow field may be expected to scale according to $L \sim L_0 e^{\lambda t}$, while due to conservation of mass, it may be expected to thin normal to the stretching direction according to $W \sim W_0 e^{-\lambda t}$. The increase in interfacial area and the reduction in striation thickness serve to further improve the mixing process by either enhancing diffusion between miscible components, or via a breakup process leading to drop formation in immiscible systems.[25–27]

In macroscopic flows, chaotic mixing is often generated using temporally controlled moving boundaries as a driving force, an approach sometimes referred to as active mixing.

a)Author to whom correspondence should be addressed. Telephone: (301) 975-6761. Fax: (301) 975-4924. Electronic mail: frederick.phelan@nist.gov.
b)Present address: Polymer Physics Section, Code 6120, U.S. Naval Research Laboratory, 4555 Overlook Avenue SW, Washington, D.C. 20375-5342. Electronic mail: jai.pathak@nrl.navy.mil.

However, this is not easily replicated in microfluidics, as production of miniature devices with moving boundaries can be expected to be unduly expensive compared to traditional microfluidic fabrication techniques, and in practical terms, more difficult to control. Given this limitation, generation of chaotic flow in the laminar channel flows inherent to microfluidic devices requires either geometric or some other means of temporal manipulation of the flow.[6,10] A number of different methods utilizing these principles have been applied to enhance mixing in microfluidic devices by creating or attempting to create chaotic flow fields. Devices that rely on geometric manipulation are generally called passive mixers, and some examples include patterned surfaces,[28–31] sinusoidal and serpentine flows,[32–36] and split and recombine flows;[37–39] devices that rely on temporal manipulation are called active mixers with some examples being exploitation of secondary flows[40–44] and oscillatory flow.[45–51]

A summary of heuristics for generating chaotic flow is listed in Ottino et al.[6] In application to the present problem, probably the most important of these is the condition that the flow streamlines at successive times, say t and $t+\Delta t$, intersect each other in the flow domain. Linked twist map (LTM) flows, such as the "blinking vortex,"[22] in which the streamlines of two annular regions intersect each other, are an example of this.[5] In this work, we consider application of the "crossing-streamline" principle to conduct a numerical study of chaotic mixing in microfluidic channel geometries that have fixed boundaries, in which chaotic conditions are achieved via temporal manipulation using oscillatory boundary conditions.[45–51] The seminal works of Truesdell et al.,[45] Tabeling et al.,[46,47] and Mezic et al.,[49] are encompassed here as limiting cases of a family of such flows.

The crossing streamlines utilized in this study are distinctly different from the intersecting annular streamlines of an LTM. Rather, we consider the case of intersecting channels, the simplest case of which is a cross-flow mixer (CFM) depicted in Fig. 1(a). Defining a Strouhal number as St $=U/L\omega$, where U, L, and ω are the characteristic velocity, length, and frequency, respectively, the results indicate that for purely oscillatory flow, chaotic mixing is achieved in the CFM starting at about a Strouhal number of $O(1)$, and that the mechanism for chaos is a type of tendril-whorl (TW) flow,[3,12] a model flow known for the generation of chaotic mixing. The CFM may be viewed as the simplest prototype flow for producing chaotic flows in purely oscillatory motion (i.e., zero net throughput flow) in channels. There are a number of ways in which the CFM mixing mechanism may be exploited to produce a well-mixed throughput stream. As an example, we consider superimposing a lateral throughput flow with the oscillatory cross-flow motion in a configuration called the star-cell, depicted in Fig. 9.

A kinematics-based approach is used to study the mixing process in these cells. Flow is modeled via numerical simulation of the unsteady Navier–Stokes equations. Using the kinematics obtained from the simulation, the deformation of material lines and blobs composed of passive tracer particles is used to identify chaotic regions and quantify the degree of mixing. The analysis proceeds as follows. First, we outline the parameters and numerical techniques used to analyze the
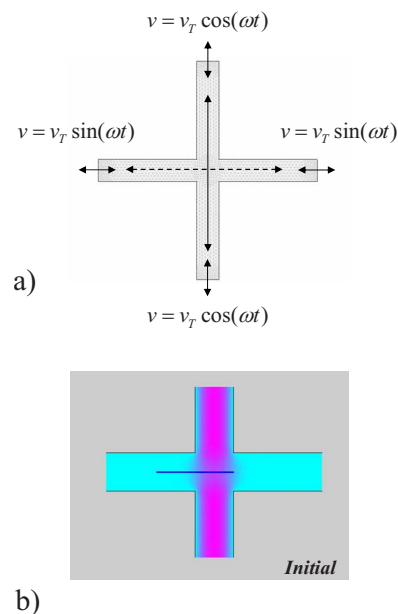

FIG. 1. (Color online) (a) Flow geometry and boundary conditions for the cross flow mixer (CFM). The channel widths were scaled to unity for all calculations. (b) Initial condition for material line stretch calculations pictured in Figs. 2 and 3. The line consists of 25000 individual particles and lies along the x axis between $[-1.5, 0.5]$.

flow. Then, confined mixing produced by purely oscillatory motion in the CFM is modeled. This allows identification of parameter regimes that are viable for producing chaotic mixing and enables us to identify the TW flow mechanism. Finally, the effect of combining a fixed throughput flow with oscillatory motion in the star-cell configuration as a means for generating continuous mixing is examined. It is found that a peak degree of mixing equal with that obtained for the purely oscillatory case can be achieved, indicating a synergy between the throughput and oscillatory motion under certain conditions. Some simple residence time distribution observations are employed to help explain some of the other system behavior. In the discussion, we examine the relationship of the mixing mechanism in the CFM and star-cell configurations to those in other oscillatory flows, particularly that of Tabeling et al.[46,47] and Mezic et al.,[49] and we show that TW flow is also inherent to other oscillatory flows, but that the mechanism can occur by either continuous or discrete means. This should lend insight to the future design of oscillatory flow mixers.

MODELING

The governing equations used to model the flow are the unsteady Navier–Stokes equations together with the incompressible condition

$$\rho\frac{\partial \underline{v}}{\partial t} + \rho\underline{v}\cdot\nabla\underline{v} = -\nabla p + \eta\nabla^2\underline{v}, \tag{2}$$

$$\nabla\cdot\underline{v} = 0, \tag{3}$$

where $\underline{v}$ is the velocity, p is the pressure, and η and ρ are the viscosity and density, respectively. Numerical solutions were

obtained using the commercial[52] finite-element package COMSOL MultiPhysics (COMSOL MP).[53]

To evaluate the ability of a given flow configuration to produce chaotic motion, the deformation of material lines and blobs composed of passive tracer particles were tracked in a manner analogous to flow experiments using tracer dyes. Particle plots were obtained using MATLAB[54] scripting codes with the exported COMSOL MP solution, where the rate of change of the individual particle positions is governed by the Eulerian velocity field according to

$$\frac{dx}{dt} = v_x(x,y,t) = \frac{\partial \psi}{\partial y},$$

$$\frac{dy}{dt} = v_y(x,y,t) = -\frac{\partial \psi}{\partial x}.$$

$$(4)$$

Two types of particle tracking analyses were conducted: single and multispecies. Single-species tracking is used to identify chaotic flow by three means. First, the equations describing the particle trajectories in 2D fluid flow formally fit the form of a Hamiltonian dynamical system in which the stream function, $\psi = \psi(x,y,t)$, acts as the Hamiltonian.[9] In such systems, chaotic regions are separated from nonchaotic regions along well-defined lines called Kolmogorov–Arnold–Moser (KAM) curves.[24] Thus, the particle plots serve as qualitative indicators of chaotic flow kinematics by identification of regions of homogeneous particle dispersion within the flow domain. A second qualitative signature of chaos related to the visual particle dispersion is ergodicity.[55] That is, no matter what initial configuration of particles is chosen, after a large number of cycles, the final states are indistinguishable from one another. A final semiquantitative signature of chaos comes from monitoring the growth of a material line. Exponential stretch of material lines is a characteristic of chaotic systems,[3] and may be used to infer the existence of chaotic kinematics. The exponent in this case can be thought of as a "finite time" or "effective" Lyapunov exponent.

Multispecies particle tracking is used to define a quantitative degree of mixing based on the concept of mixing entropy. The procedure followed here is the same as is defined in Kang and Kwon,[56] and has been employed in a number of studies, e.g., Stone and Stone.[36] In this method, a mixing zone is specified and divided into a number of discrete flow cells. The mixing zone may encompass either all or part of the flow domain. A number of particle species (distinguished visually by color) are then introduced into the flow and allowed to mix. A mixing entropy for the particles may be defined as

$$S = -\sum_{i=1}^{N_c} \left(w_i \sum_{j=1}^{N_s} (n_{i,j} \log n_{i,j}) \right),$$

$$(5)$$

where N_c is the number of flow cells, N_s is the number of species, $n_{i,j}$ is the fraction of species j in the flow cell i, and w_i is a weighting function with a value of zero in cells that contain only a single species, and unity in cells that contain multiple species. Based on this, a degree of mixing may be defined as

$$D_m = \frac{S}{S_{\max}},$$

$$(6)$$

where $S_{\max}$ is the maximum obtainable entropy for the system and is given by

$$S_{\max} = N_c \log \frac{1}{N_s}.$$

$$(7)$$

The value of D_m is thus a dimensionless value bounded by [0,1], where a value of zero represents a complete segregation of species, and unity represents perfectly uniform mixing. It was found by trial and error that one issue with this method is the number of flow cells used to discretize the mixing zone. If the discretization is too coarse, an artificially high degree of mixing is obtained; if it is too fine, an artificially low degree of mixing may be obtained. The procedure followed here was to refine the number of flow cells until successive calculations yielded ostensibly the same result. In general, it was found that the calculation converged relatively quickly, and the exact number of cells used is reported below on a case by case basis.

An issue in any particle tracking scheme is collision of particles with the boundary, and since the streamlines do not intersect the boundary, this must be regarded as an integration error. Nevertheless, it is difficult to avoid in some degree when the flow becomes strongly chaotic. Boundary collisions do not strongly influence the overall dispersion patterns seen in any of the simulations (although some fine details may vary on a localized scale), however they have to be completely eliminated in order to calculate an effective Lyapunov exponent, and highly minimized ($<0.1\%$) in the degree of mixing calculations. In the present work, boundary collisions become an issue when the Strouhal number is about double the value at which the transition to chaos occurs. To eliminate collisions, unacceptable calculations were first repeated with greater temporal resolution, and if that proved insufficient, greater spatial resolution as well. Thus, the size of the time step used in the simulations varied anywhere from 80 to 800 time steps per sinusoidal cycle, with a greater number being used as the Strouhal number increased.

The majority of the calculations were carried out on a Dell PC workstation, with a 3 GHz processor and 2 Gb of RAM. Computation times for the finite-element calculation of the flow field were very robust, with the longest CPU time being on the order of 20 min. Computation time for particle dispersion plots and computation of stretching exponents depended greatly on how many time steps were used. Approximately four hours per plot were needed for a 15 cycle calculation, at 400 time steps per cycle. By far the degree of mixing plots calculations was the most time consuming of all the analyses, approximately three to four times longer than the particle plots for a grid of 400 flow cells due to the time-consuming nature of interpolating particle positions on the mixing grid.
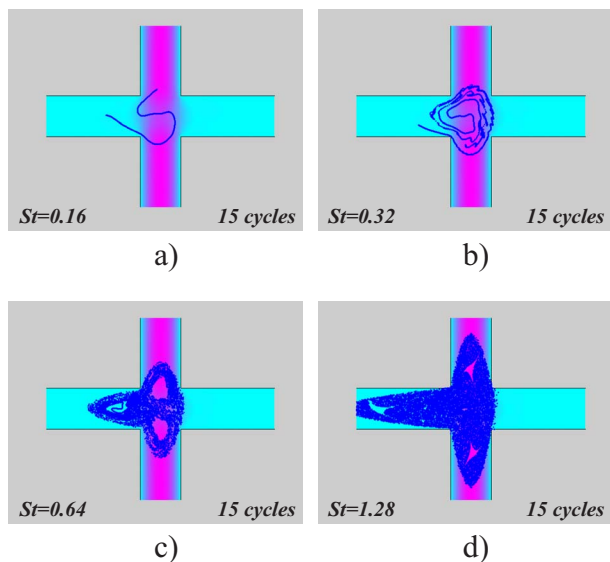
FIG. 2. (Color online) Stretching of a material line in the CFM as a function of Strouhal number after 15 cycles for the initial condition shown in Fig. 1(b). (a) St=0.16, (b) St=0.32, (c) St=0.64, (d) St=1.28 (enhanced online).

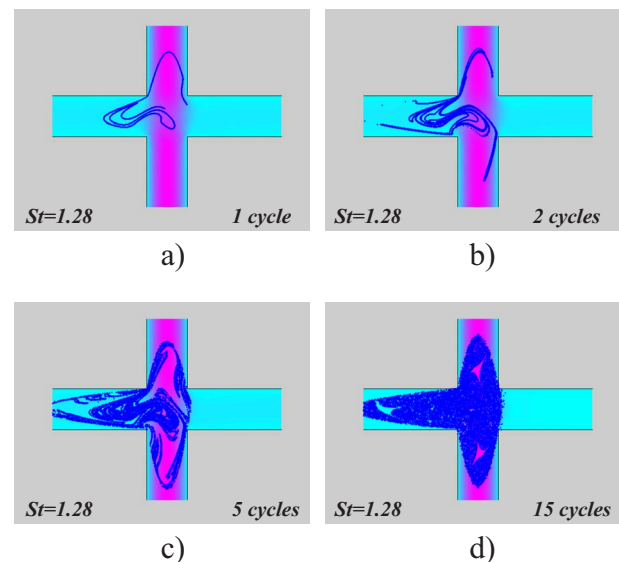
FIG. 3. (Color online) Stretching of a material line in the CFM for St =1.28 as a function of cycle time. (a) $N=1$, (b) $N=2$, (c) $N=5$, (d) $N=15$.

CONFINED MIXING: CROSS-FLOW MIXER (CFM)

Flow geometry and boundary conditions

The CFM geometry with boundary conditions is shown in Fig. 1. The figure indicates that the flow oscillates in the vertical direction according to a cosine function, with oscillations in the horizontal direction being 90° out of phase. Thus, the oscillatory flow in the system is balanced so as not to produce any net throughput flow, and successive sets of temporal streamlines cross normal to each other every quarter period at the center of the geometry (as required for chaos per the crossing-streamline principle), also indicated in the figure. The velocity profile at all the inlets is assumed to be parabolic, where the magnitude of the maximum oscillatory velocity component is given by v_T. The sinusoidal oscillations imposed on the system are characterized by an angular frequency $\omega=2\pi/T$, where T is the period. Based on this, the dimensionless groups governing the flow are the Reynolds number, $Re=\rho v_T L_c/\eta$, and a Strouhal number, $St=v_T/L_c\omega$, where L_c is a characteristic length taken here to be equal to the channel width. For all calculations, L_c and ρ were scaled to unity, the frequency was set at $\omega=\pi/2$, and the viscosity was set to $1000\cdot\rho$. Since $\rho/\eta=0.001$, $L_c=1$, and the maximum velocity used in any calculation is $v_T=5$ at St=3.2, the Reynolds number is always small enough that inertia can be considered to be negligible.

Onset and characteristics of chaotic flow

The basic characteristics of the deformation induced by the flow as a function of Strouhal number in the CFM are shown in Fig. 2. This depicts results for the stretching of a material line after $N=15$ cycles (where the absolute time $t=N^*T$) for successively doubling St values of St $=[0.16, 0.32, 0.64, 1.28]$. The line is composed of 25000 points, and is initially stretched along the x axis between $[-1.5, 0.5]$ as shown in Fig. 1(b). In Fig. 2(a), for St=0.16,

the line shows neither a high degree of stretching nor evidence of chaotic behavior, but it has deformed into a characteristic S shape, which is a signature of the mapping induced by this flow field. For St=0.32, in Fig. 2(b), an S-type folding is again evident, but in this case the line has wrapped up upon itself several times, as evidenced by striation layers. In Figs. 2(c) and 2(d), traces of the initial line are no longer apparent, and a transition to seemingly chaotic behavior is evident. In the Appendix, it is shown that the chaotic region continues to grow in size as St increases in a pattern mirroring that seen in Fig. 2(d), although additional islands appear. Videos of the deformation depicted in Figs. 2(b) and 2(d) are also available. *N.B.*, in this plot, and all that follow, the background color map indicates the magnitude of the velocity at the current value of time, with magenta indicating a maximum, and light blue a minimum.

Details of the transition for St=1.28 are examined in Fig. 3, which shows the stretch of the line at times of $N =[1, 2, 5, 15]$ cycles. The figure indicate that the line continually stretches and folds upon itself, and gradually, the individual particles become scattered within the region over which the line is folded. A semilog plot of (L/L_0) vs time for the simulation shown in Fig. 3 is shown in Fig. 4, where L_0 is the initial length of the line. The plot shows that the data very closely fit an exponential relationship with an exponent value of $\lambda=0.41$, indicating a positive "effective" Lyapunov exponent. The collective behavior exhibited in Figs. 3 and 4 is characteristic of that in a Hamiltonian system in which material lines undergo exponential stretching and folding leading to particle dispersion,[24] and we conclude that the motion induced by the intersecting sinusoidal oscillations is chaotic.

Using the multiparticle analysis method outlined above, the degree of mixing was calculated for the CFM at a range of Strouhal numbers. The initial condition depicting two rectangular patches of "red" and "blue" particles is shown in Fig. 5(a). Each patch consists of 10201 particles. The patches
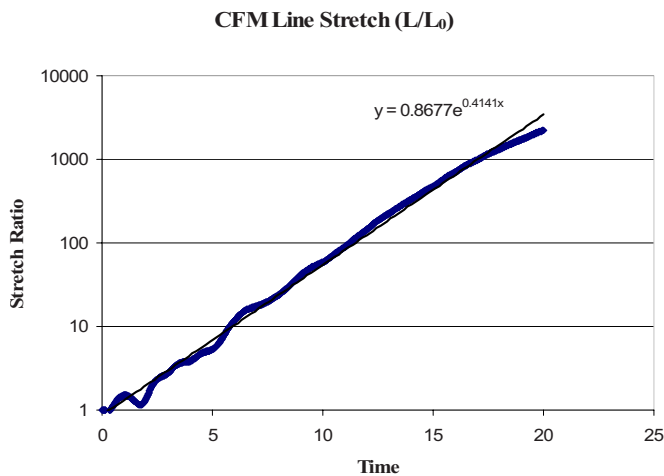
CFM Line Stretch (L/L₀)

FIG. 4. (Color online) Semilog plot of the line stretch (L/L_0) vs time for the stretching of a material line in the CFM at St=1.28. The line shows a constant exponential stretch rate of $\lambda=0.41$.

Cross Flow Mixer

FIG. 6. (Color online) Degree of mixing as a function of cycle time obtained from multispecies mixing entropy calculations in the CFM for various values of the Strouhal number.

are initially positioned on opposite sides of center of the flow channel to mimic the impingement of different species; e.g., see Refs. 45–47. The mixing zone is defined as the central square stagnation region of the geometry, and for all data reported here it consisted of a 20×20 grid of flow cells. Figure 5(b) shows the mixing of the blobs after 30 cycles for St=1.28. The particles appear homogeneously dispersed except for a small island region in the center. A plot of degree of mixing versus cycle time for St=$[0.96,1.28,1.6,1.92]$ is

shown in Fig. 6. The plot shows that the degree of mixing increases with the Strouhal number up to a peak value of approximately $D_m\approx0.91$ at St=1.28, after which it begins to decline due to the growth of the island in the center region of the geometry.

Tendril-whorl flow mechanism

The mechanism by which chaotic flow is generated can be ascertained in part by examining the initial stretching of the line in the CFM at quarter cycles times of $N=[0.25,0.5,0.75,1]$, as shown in Fig. 7, again for St=1.28. The initial deformation of the line, shown in Fig. 7(a), stretches the line nonuniformly in the y direction creating a horseshoe-shaped fold. Labeling two points near bends in the line as "a" and "b," the relative positions of these points are tracked in the next three frames, Figs. 7(b)–7(d). The figures show that an arrow drawn between the two points undergoes
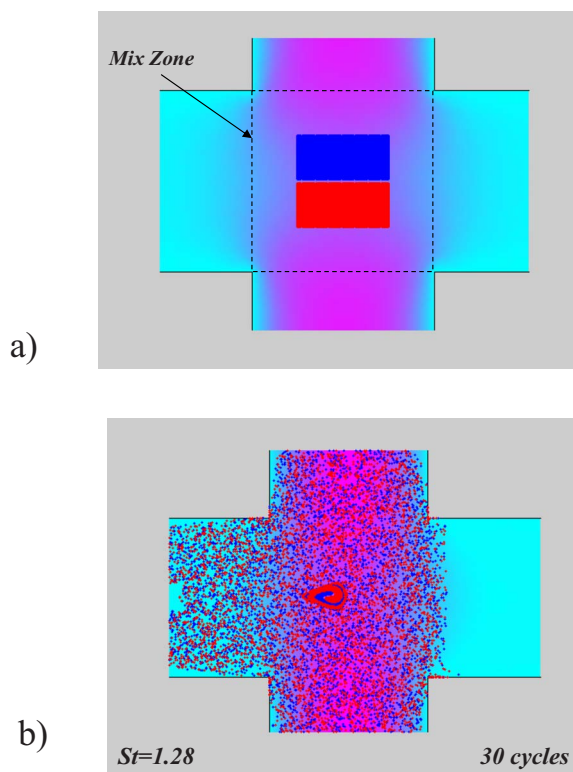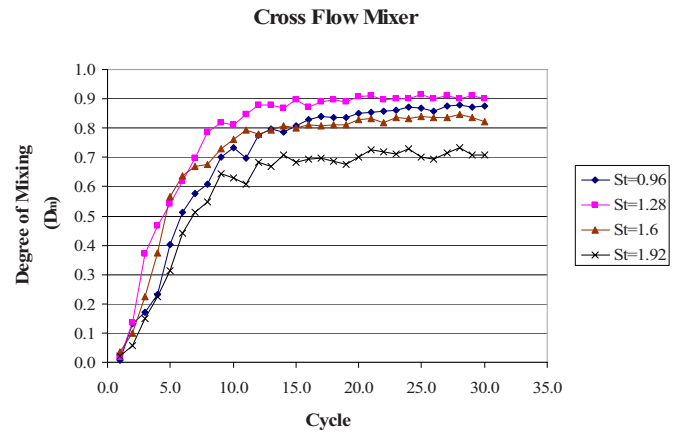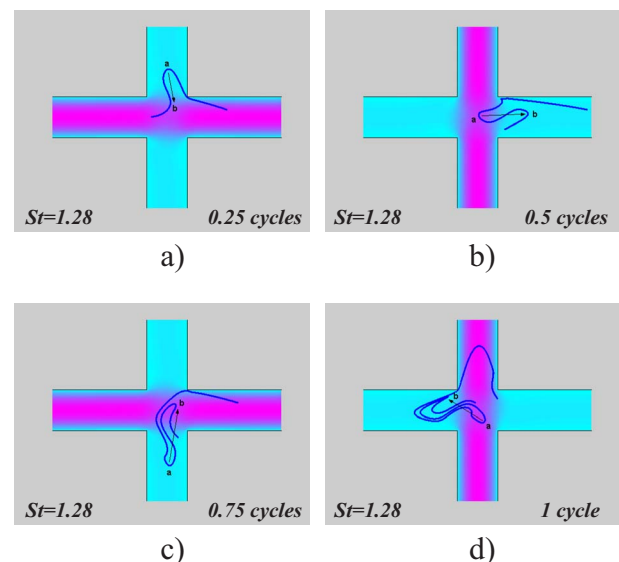

FIG. 5. (Color online) (a) Initial condition for multispecies mixing calculations in the CFM. Each rectangular patch consists of 10201 particles. The mixing zone is defined as the square center region of the geometry. (b) Multispecies mixing in the CFM for St=1.28 after 30 cycles.

FIG. 7. (Color online) Illustration of the tendril-whorl flow mechanism in the CFM at St=1.28 as shown by the initial stretching of a material line at quarter cycle times. (a) $N=\frac{1}{4}$, (b) $N=\frac{1}{2}$, (c) $N=\frac{3}{4}$, and (d) $N=1$.
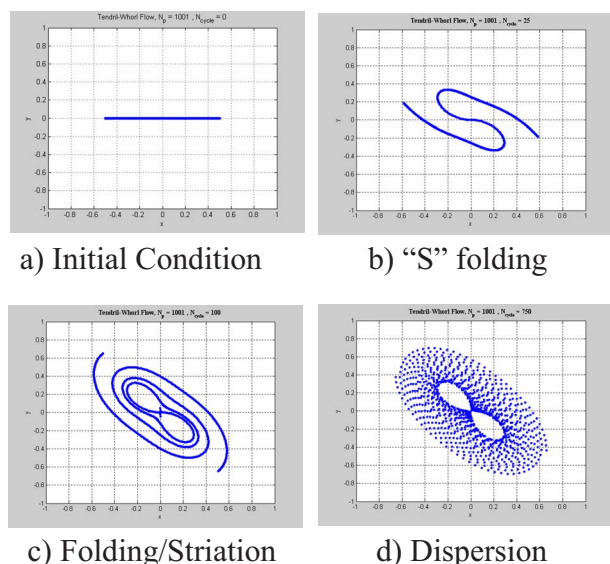
a) Initial Condition   b) "S" folding

c) Folding/Striation   d) Dispersion

FIG. 8. (Color online) The stretching of a material line of 1000 particles in a theoretical tendril-whorl flow with the kinematics $v=(\dot{\varepsilon}x,-\dot{\varepsilon}y)$ for $0<t<T_{ext}$ and $v_{\theta}=-Br^2e^{-r}/T_{rot}$ for $T_{ext}<t<T_{ext}+T_{rot}$, for $\dot{\varepsilon}=0.1$, $B=0.5$, $T_{ext}=1$, and $T_{rot}=1$. (a) Initial condition, (b) 25 cycles, (c) 100 cycles, (d) 750 cycles.

a continuous counterclockwise rotation as cycle time increases. Thus, a twofold deformation mechanism is present in the flow: portions of the material line are stretched in the channels via shear flow, while the timing of the shear flow oscillations acts to continuously rotate the line counterclockwise.

A flow that combines periodic stretching and rotation to produce chaotic mixing is characteristic of a tendril-whorl (TW) flow.[3,12] Characteristics of a specific tendril-whorl flow using kinematics from Ottino[3] are shown in Fig. 8. In addition to the common mechanism shown in Fig. 7, the results for the CFM in Fig. 3 show at least three qualitative common characteristics with the theoretical TW flow: an initial stage in which horseshoe- or S-shaped folds are generated; a second stage in which the line continually folds upon itself creating striation layers; and a final long-time behavior in which the initial line structure is no longer evident and the particles become dispersed within the region in which the stretching and folding occurs. The sum of these qualitative similarities strongly suggests that the mechanism for mixing in the CFM is indeed a type of TW flow.

CONTINUOUS MIXING: STAR-CELL GEOMETRY

Geometry and boundary conditions

In order make use of the CFM mixing mechanism in a continuous throughput operation, the star-cell geometry shown in Fig. 9 is introduced. In this flow, a continuous throughput channel flow is superimposed on an oscillatory cross flow with the idea being for the oscillatory flow to provide chaotic mixing (as it does in the CFM), and for the continuous flow to carry the mixed species downstream. The adjacent arms of the star-cell are arranged at 60 deg to one another. In the orientation shown, the horizontal arms represent the throughput direction (from left to right), and the
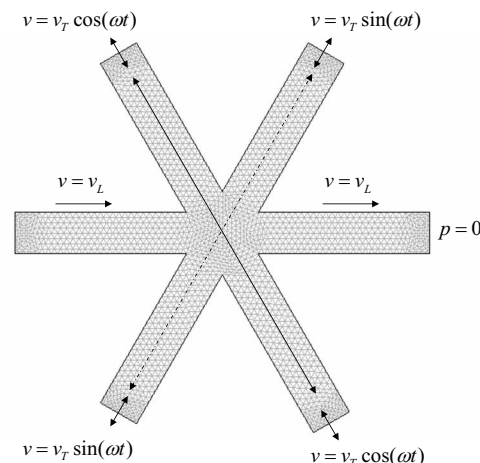

FIG. 9. Flow geometry and boundary conditions for the star-cell mixer.

transverse arms are used to mix the fluid via oscillatory motion. Flow in the transverse channels is cross-balanced as per the CFM, with the upper left channel and lower right channel oscillating according to a cosine function, and the upper right and lower left oscillating according to a sine function. This cross-balancing creates a streamline crossing point at the center of the cell every quarter cycle, as indicated. A steady lateral component of velocity is indicated along the horizontal axis of the channel.

As for the CFM, in all the calculations, the inlet velocity profiles were assumed to be parabolic, with the maximum velocity of the oscillatory velocity component indicated by v_T, and the maximum velocity of the lateral throughput velocity indicated by v_L. The values of ρ, η, L_c, and ω were the same as used for the CFM. The introduction of the lateral velocity component introduces another dimensionless group to the system. While it is natural to introduce the velocity ratio $R_v=v_L/v_T$, it was found in the course of analysis that it is more useful to characterize results in terms of the product of the Strouhal number and the velocity ratio, which is itself dimensionless throughput velocity given by $U=\text{St}\cdot R_v=v_L/L_c\omega$.

Oscillatory flow

The oscillatory flow channels of the star-cell are oriented at a slightly different angle than they are for the CFM. Thus, we first analyze mixing for purely oscillatory motion to show that the mixing characteristics are not significantly altered by the angle change, and to establish a baseline against which throughput mixing can be compared.

The characteristics of the deformation of a single species material line induced by purely oscillatory flow in the star-cell are shown in Figs. 10 and 11. The line is composed of 25000 points, and is initially centered along the x axis from $[-1,1]$. Figure 10 depicts results for the stretching of the line after $N=15$ cycles, for successively doubling St values of St$=[0.16,0.32,0.64,1.28]$. Figure 11 shows the time-dependent deformation of the line at times of $N=[0,2,5,15]$ cycles for the case of St$=1.28$, and is available as a video in supplementary material. It is apparent that the
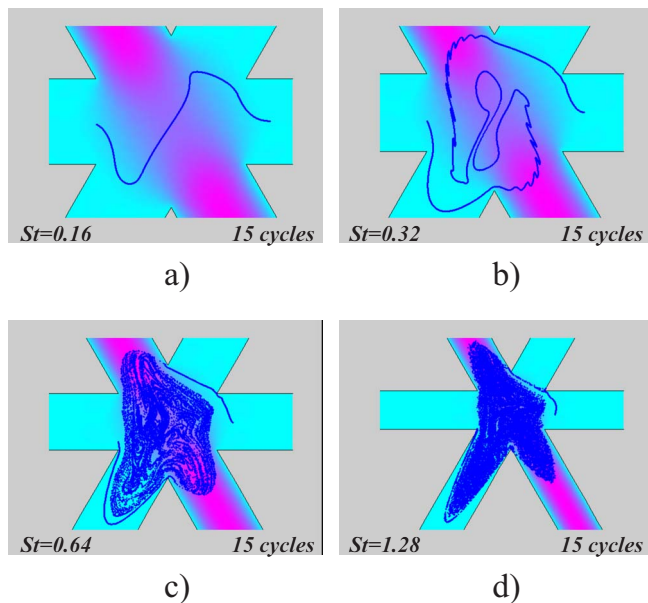
FIG. 10. (Color online) Stretching of a material line in the star-cell as a function of Strouhal number after 15 cycles for the initial condition shown in Fig. 11(a). The line is composed of 25000 points, and is initially centered along the x axis between $[-1,1]$. (a) St=0.16, (b) St=0.32, (c) St=0.64, (d) St=1.28.

stretching mechanism that leads to chaotic behavior in the CFM with increasing Strouhal number is also present in the star-cell, cf. Figs. 2 and 10 and Figs. 3 and 11. For both cases, the low St behavior is characterized by the introduction of S-shaped folds into the line, followed by a folding/striation layer regime at intermediate St, and ultimately, a dispersion regime at high St. In addition, examination of the time sequences in Fig. 11 illustrates the same mechanism for chaotic mixing in which stretching and folding lead to particle dispersion. The effective Lyapunov exponent calculated
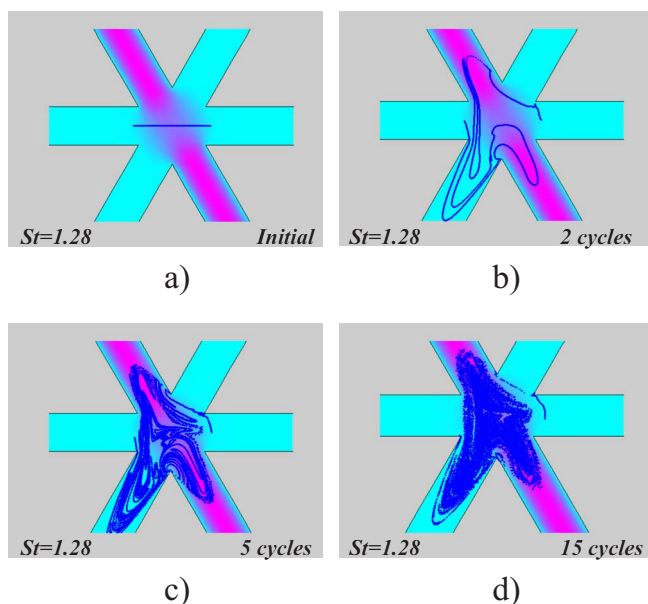

FIG. 11. (Color online) Stretching of a material line in the star-cell for St=1.28 as a function of cycle time. (a) $N=0$, (b) $N=2$, (c) $N=5$, (d) $N=15$ (enhanced online).
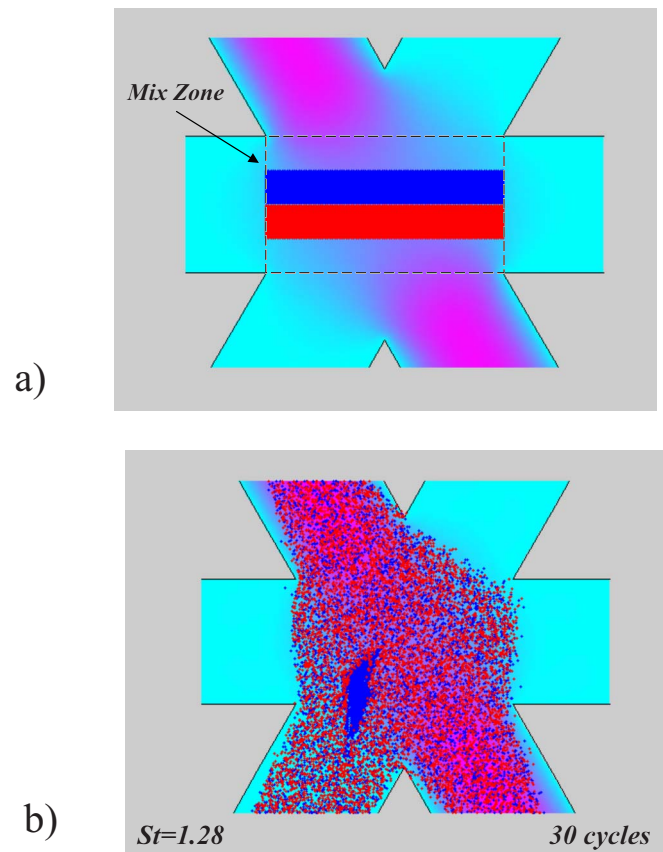

FIG. 12. (Color online) (a) Initial condition for multispecies mixing calculations in the star-cell. Each rectangular patch consists of 10201 particles. The mixing zone is outlined as the center rectangular region of the geometry. (b) Multispecies mixing in the star-cell for St=1.28 after 30 cycles.

from the change in length of the line at St=1.28 (i.e., the same Strouhal number as used in the exponent calculation for the CFM, cf. Fig. 4) yields a value of $\lambda=0.25$ as shown in Fig. 16 (*n.b.*, for the exponent calculation a slightly shorter line initially centered along the x axis from $[-0.25,0.25]$ was used). The dispersion patterns seen in Figs. 10 and 11, and the positive stretching exponent calculated from the line stretch, indicate that the flow is chaotic.

Results from multispecies particle tracking simulations to characterize the degree of mixing are shown in Figs. 12 and 13. The initial condition for the particles is shown in Fig. 12(a). Each rectangular patch consists of 10201 particles. The position of the mixing zone is also indicated in the figure and consisted of a 20×20 grid of flow cells. Figure 12(b) shows an example of the mixing of the two groups for St $=1.28$ at $N=30$ cycles. It is evident that the particles are very homogeneously dispersed, except for the island region near the center. The degree of mixing for a range of Strouhal numbers is shown in Fig. 13. The peak degree of mixing achieved in the purely oscillatory star-cell is approximately $D_m \approx 0.9$, and occurs at about St=1.28, which is very similar to the results for the CFM. However, the drop in degree of mixing with increasing Strouhal number for the star-cell is not nearly as sharp as it is for the CFM, in part because the size of the island near the center grows at a slower rate. For
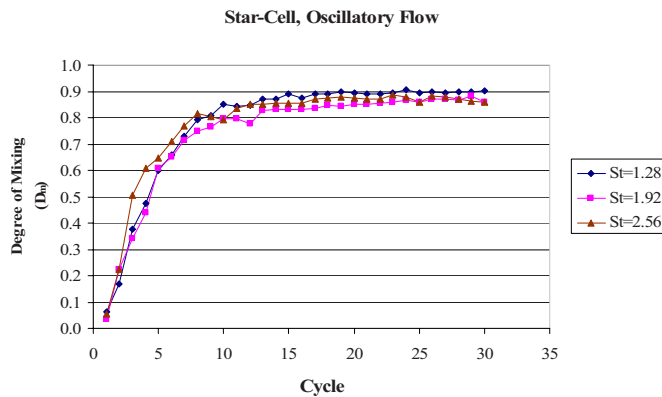
Star-Cell, Oscillatory Flow

FIG. 13. (Color online) Degree of mixing as a function of cycle time obtained from multispecies mixing entropy calculations in the star-cell for various values of the Strouhal number.

all cases, it is reasonable to conclude that greater than 10 but closer to 15 cycles are needed to effectively mix two impinging fluid streams.

The mechanism for chaotic flow in the CFM was shown to be a type of tendril-whorl flow, in which portions of the material line are stretched in the channels via shear flow, while the timing of the shear-flow oscillations continuously rotates the line counterclockwise. We show this for the star-cell as well in Fig. 14, again at St=1.28. The initial position of the line is shown in Fig. 14(a). Two points on the line are labeled as "a" and "b," and the relative positions of these points are tracked in the next three frames, Figs. 14(b)–14(d), which correspond to cycle times of N=0.5, 1.5, and 2.75. The figures show that an arrow drawn between the two points undergoes a continuous counterclockwise rotation as cycle time increases, where the rate of rotation at this Strouhal number is about one transverse channel per cycle.
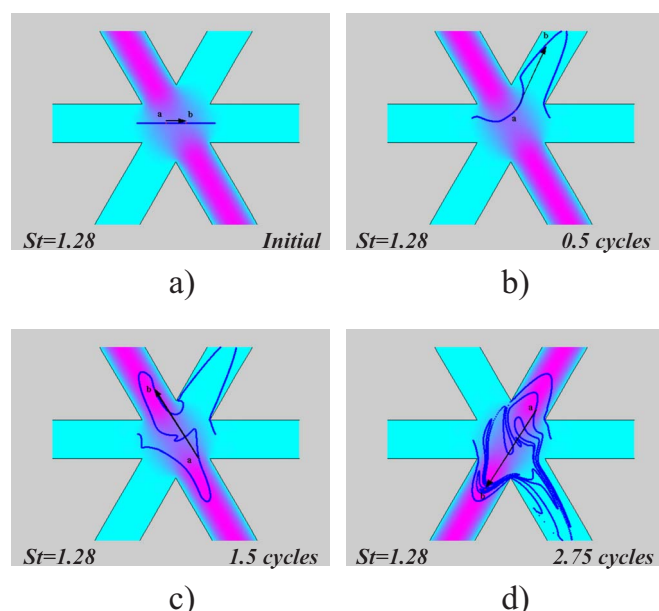

FIG. 14. (Color online) Illustration of the tendril-whorl flow mechanism in the star-cell geometry at St=1.28 as shown by the stretching of a material line at various cycle times. (a) N=0, (b) N=0.5, (c) N=1.5, and (d) N=2.75.
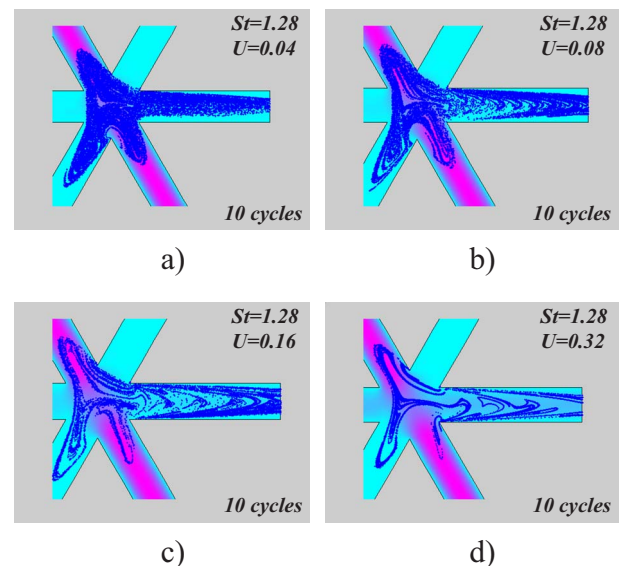

FIG. 15. (Color online) Particle dispersion as seen in the stretch of a material line in the star-cell geometry for St=1.28 at a cycle time of N=10 as a function of the dimensionless throughput velocity (U). (a) U=0.04, (b) U=0.08, (c) U=0.16, and (d) U=0.32.

Continuous mixing at fixed St

To evaluate the effect of combining throughput flow with oscillatory motion, line stretch calculations were performed for the star-cell geometry, at fixed values of St, and increasing values of the dimensionless throughput velocity U. For the calculations shown, the Strouhal number was fixed at St=1.28 as this was the near-optimal value for mixing in both the CFM and the star-cell with zero throughput flow.

Figure 15 shows dispersion patterns based on the deformation of a material line in the star-cell geometry, for St =1.28 and values of U=[0.04,0.08,0.16,0.32]. The initial condition is the same as for Figs. 10 and 11. Ideally, the dispersion pattern would uniformly fill the entire downstream space of the effluent, just as they fill the center region of the flow cell in purely oscillatory motion. However, some deviations from the ideal case scenario are evident. At the smallest value of U, while the dispersion pattern is uniform, particle segregation to the upper side of the downstream channel is evident. As U further increases, the segregation effect disappears and the particles in the effluent more homogeneously fill the cross section of the output channel. However, the disappearance of segregation is accompanied by an increase in the size of the unmixed island regions in the downstream dispersion pattern, with the size of the islands increasing with throughput rate. Thus, for a fixed Strouhal number, there appears to be an optimal throughput ratio at which segregation is eliminated, and islands are minimized. By visual inspection, at a fixed value of St =1.28, the optimal value of U for the star-cell appears to be either U=0.08 [Fig. 15(b)] or U=0.16 [Fig. 15(c)].

Figure 16 compares plots of log(L/L_0) vs t for the star-cell geometry at St=1.28 for the cases U=0 and U=0.16, the latter for the initial condition shown in Fig. 15. In the plot for the throughput cases, there is a relatively low slope region at
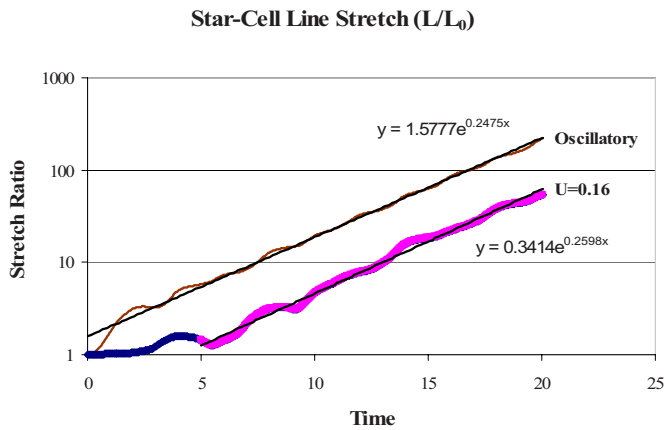
FIG. 16. (Color online) Semilog plots of (L/L_0) vs time in the star-cell geometry at St=1.28 for purely oscillatory and continuous flow conditions. (a) $U=0$, (b) $U=0.16$.
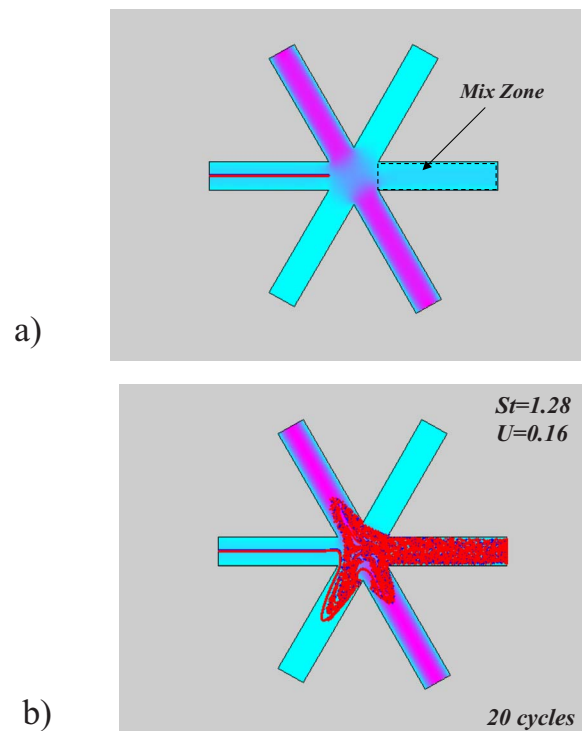

FIG. 17. (Color online) (a) Initial condition and mix zone for multispecies mixing calculations in the star-cell under continuous flow conditions. Each initial line consists of 1000 particles of a single species and are positioned $\pm\delta$ above and below the centerline, respectively, with $\delta=0.01$ (blue above, red below). In addition, one new particle of each species was added to the flow at each time step along the inlet boundary at points $\pm\delta$ above and below the injection centerline. The mixing zone is outlined and is defined as the outlet flow channel of the geometry. (b) Multispecies mixing in the star-cell for St=1.28 and $U=0.16$ after 20 cycles (enhanced online).

the start that corresponds to the convection of the downstream particles into the mixing region, followed by a rapid increase in slope when the particles have fully entered the mixing region. The plot for the oscillatory flow portion fits an exponential relationship in which the effective Lyapunov exponent has a value of $\lambda=0.26$. This is for all intents and purposes unchanged relative to the purely oscillatory case, as can also be seen by comparing the slopes in the figure. The dispersion patterns of Fig. 15 and the positive exponent of Fig. 16 indicate that chaotic flow is maintained, even under throughput conditions.

Continuous mixing at fixed throughput rate

To quantitatively evaluate the degree of mixing of two different fluid streams in the star-cell under continuous flow conditions, multispecies particle mixing was modeled for fixed values of the dimensionless throughput velocity U and increasing values of St. The initial condition and mix zone used to evaluate the degree of mixing for these simulations are shown in Fig. 17(a). The initial condition consists of two lines of particles, one blue and the other red, each with 1000 points, and each positioned slightly above and below the injection midline, respectively. In addition to the initial particles, points along the inlet boundary but on opposite sides of the injection midline allow for the continuous injection of particles of different species. The mix zone was taken to be the entire length of the outlet channel, and consisted of a 40×10 grid of flow cells. The degree of mixing is computed after each sinusoidal cycle, which we deem sufficient due to the fact that the oscillations do not significantly affect the downstream particle dispersion. An example of a multispecies result for $U=0.16$ and St=1.28 is depicted in Fig. 17(b), at a cycle time of $N=20$. The effluent appears quite uniform with respect to species.

The degree of mixing across a range of Strouhal numbers at values of $U=[0.16,0.32]$ is shown in Figs. 18(a) and 18(b), respectively. For these calculations, one new particle of each species was added to the flow at each time step at the points $[-5,0.01]$ and $[-5,-0.01]$, respectively. The maximum values of D_m for each case are plotted in Fig. 19. The

calculations show that at fixed throughput, increasing the Strouhal number drives the degree of mixing up to a maximum, at which point it levels off to an ostensibly steady plateau value that is slightly lower but commensurate with the maximum. For $U=0.16$, the maximum is $D_m=0.91$ and occurs at St=1.28, with a plateau value on the order of $D_m\approx0.9$. For $U=0.32$, the maximum is $D_m=0.81$ and occurs at St=1.92, and the plateau value is on the order of $D_m\approx0.8$.

From these data, a number of observations can be made. First, it can be seen that the maximum degree of mixing for the case of throughput flow in the star-cell for $U=0.16$ and St≥1.28 (Fig. 19) is essentially equivalent to the maximum achieved for purely oscillatory flow. Thus, these conditions can be taken to be very close to optimal. However, it is also observed that both the maximum and plateau degree of mixing values are slightly decreasing functions of the dimensionless throughput rate, and that the Strouhal number required to achieve the max/plateau level increases as U increases. Therefore, since the mixing depends on two dimensionless groups (St and U), which for a geometry of fixed size depend on three independent quantities (v_T, v_L, and ω), to maintain the 90% mixing level when changes in the actual throughput rate are required, the transverse flow rate and frequency must also be simultaneously and appropriately adjusted. If this is not done, then the degree of mixing will drop, as indicated by Fig. 19.
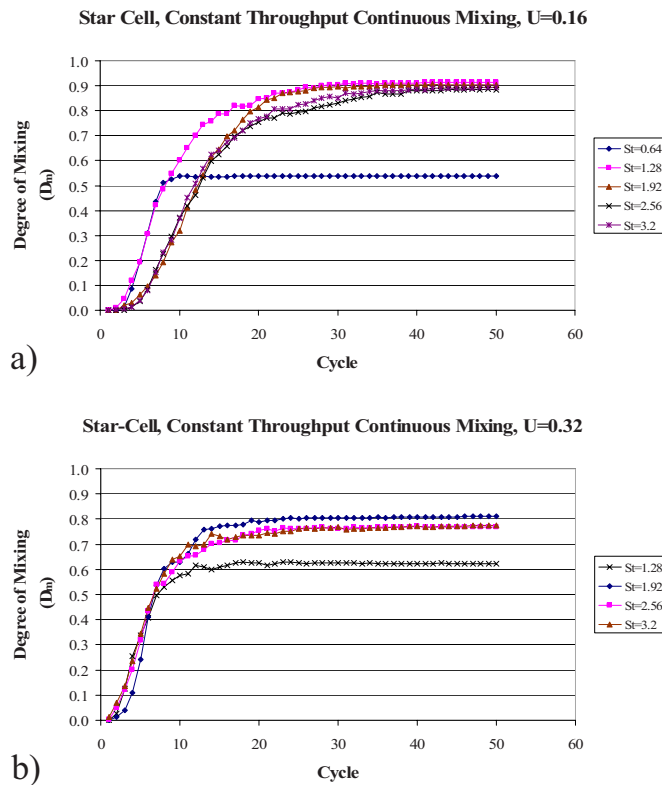
FIG. 18. (Color online) Degree of mixing as a function of cycle time obtained from multispecies mixing entropy calculations in the star-cell for fixed throughput velocity (U) and various values of the Strouhal number. (a) $U=0.16$, (b) $U=0.32$.

Another noteworthy aspect of the calculations is that combining throughput flow with the oscillatory flow appears to have a synergistic effect under some conditions. The first observation in this regard is that the maximum degree of mixing for the case of throughput flow at $U=0.16$ and St $=1.28$ is actually about 1% higher than for the oscillatory flow. Another example has to do with high St oscillations. It was shown earlier that increasing the Strouhal number past approximately St$=1.28$ has a deleterious effect on purely oscillatory mixing in both the CFM and the star-cell. However, the throughput case shows a different Strouhal number dependence in that a high degree of mixing levels can be maintained well past St$=1.28$. A plausible explanation for these
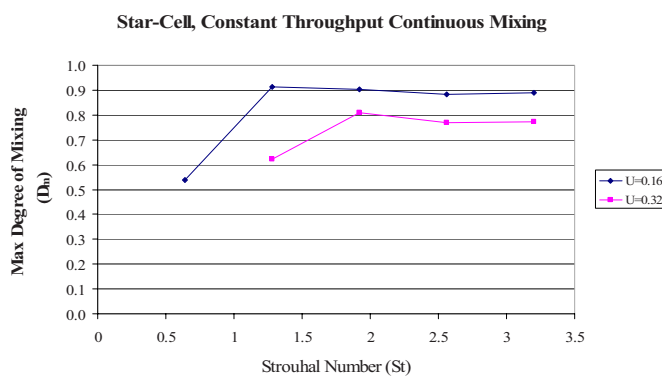

FIG. 19. (Color online) The maximum degree of mixing vs Strouhal number as a function of throughput velocity.
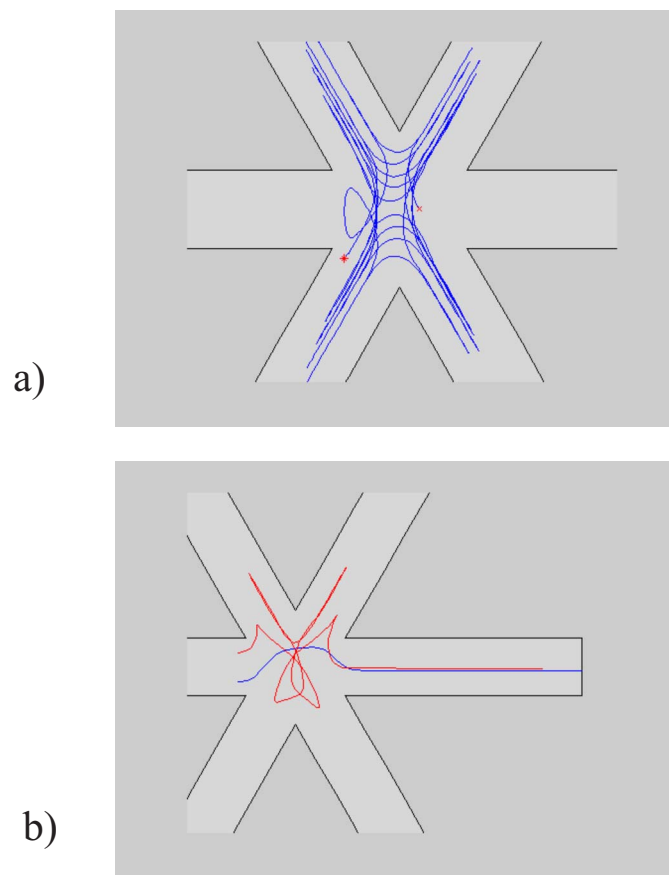

FIG. 20. (Color online) (a) Typical particle path for purely oscillatory flow in the star-cell geometry at St$=1.28$ for $N=15$ cycles. The particle is initially positioned at the "×" marker just to the right of the center of the cell, and finishes at the "*" marker at the lower left. (b) Paths of two particles entering from upstream at the same horizontal position, but separated vertically on opposite sides of the centerline in the star-cell geometry at St $=1.28$ and a finite throughput rate.

cases is that the throughput flow under some conditions acts to suppress the islands that are naturally formed under purely oscillatory conditions. This raises the speculative possibility that the use of mixed frequency or multifrequency waveforms more complex than the simple sinusoidal oscillations employed here might also be effective in increasing the maximum degree of mixing for both oscillatory and throughout flow.

Residence time distribution

Some of the behavior that is seen in the continuous mixing calculations may be explained in part by observations related to the residence time behavior of the particles. First, we examine the behavior of individual particles as they move in the central mixing region. Figure 20(a) shows a typical path of a single particle for purely oscillatory flow in the star-cell geometry at St$=1.28$ for $N=15$ cycles. The particle is initially positioned at the "×" marker just to the right of the center of the cell, and finishes at the "*" marker at the lower left. The figure indicates that the particle traverses all the transverse flow arms on a continual basis, and that the flow path is irregular and changes from cycle to cycle. It is this type of complex, nonrepeating kinematics that is respon-

sible for producing chaotic behavior for the purely oscillatory case. For the case of throughput flow, Fig. 20(b) shows the paths taken by two particles entering from upstream at the same horizontal position, but separated vertically on opposite sides of the centerline. The lower particle (depicted by the blue line) is only slightly deflected and passes quickly through to the downstream region, whereas the upper particle (red line) makes an entire orbit in the chaotic region, making passes in all four transverse channels, before flowing downstream. Initial conditions that produce particle residence times that last for multiple orbits are also possible to show. This indicates that for the case of throughput flow, the time of flight spent in the mixing regime in which particles undergo chaotic orbits follows a distribution of residence times (RTD), with some passing through quite quickly and others taking much longer. This is in contrast to the zero throughput case in which all particles spend equal amounts of time in the chaotic regime. Based on this, it seems reasonable to speculate that the general decrease in the maximum degree of mixing with increasing throughput rate may be traceable in part to the nonuniform RTD, with broadening or skewing at the low end of the distribution under certain parameter conditions (i.e., quickly exiting particles) acting as a limiting factor.

Another factor that is observed to have some effect on the mixing in the star-cell is related to the average residence time. By comparing the relative particle densities in the center mixing region in Figs. 15(a)–15(d) (which all correspond to 10 cycles) it is observed that at constant Strouhal number, the particle holdup (which is related to the average residence time) drastically decreases as the throughput rate increases. The conditions in Figs. 15(c) and 15(d) correspond to data points on the upper and lower curve in Fig. 19 at St=1.28, where the lower rate [Fig. 15(c)] has the higher degree of mixing. The decreasing holdup, therefore, is linked with a decrease in the degree of mixing. Thus, it seems reasonable to hypothesize that good mixing is observed when the Strouhal number is large enough to produce a highly chaotic flow and the average residence time is sufficient to allow enough time for the fluid elements to mix. Since the particle hold up also increases as the Strouhal number increases at constant U, this helps explain why the degree of mixing recovers to some extent for $U=0.32$ and St≥ 1.92, with full recovery not occurring, possibly due to the speculated distribution broadening with increased rate.

DISCUSSION

The primary goal in this work was to investigate the means of generating chaotic flow in microfluidic channels that are geometrically simple, where active chaotic mixing is achieved through temporal manipulation of the flow field. Because the boundaries are restricted to being simple, to achieve temporal manipulation we make use of oscillatory flow boundary conditions, similar to those cited in previous studies, but in a manner leading to a related but slightly different class of flows, as is discussed in more detail below.

Ottino and Wiggins[11] recently wrote in the context of designing optimal micromixers that, "microfluidic applica-

tions can benefit by a closer linkage and use of basic theory." In keeping with the spirit of this idea, the starting point in this work was the consideration of how the principle of crossing spatio-temporal streamlines—a necessary condition for generating chaotic flow[6]—could be applied in the context of microfluidics. Because channel flows are the inherent feature of microfluidic flows, it was reasoned that the simplest and most straightforward way to bring about the generation of crossing streamlines was through the use of intersecting channels.

The results presented here are naturally divided into two categories, the confined flow mixing achieved in the CFM, and the continuous mixing achieved in the star-cell. For the CFM, the primary goal of generating chaotic flow in a confined geometry without moving parts using the principle of spatio-temporal crossing streamlines has been realized, quite successfully. The results show that oscillatory flow in intersecting channels becomes chaotic at a Strouhal number of about unity, and that the size of the chaotic region continually increases with Strouhal number (although the overall quality of mixing does not necessarily increase due to the growth of islands). The flows are shown to be chaotic by visual inspection of particle dispersion when material lines undergo stretching and folding, and by the computation of positive "effective" Lyapunov exponents. Although it has not been specifically discussed, the ergodic property of the flow can readily be seen by comparison of dispersion patterns obtained from line stretch and multispecies blob mix calculations, cf. Figs. 3(d) and 5(b). A peak degree of mixing of about 91% is achieved in the CFM at St=1.28. This flow configuration represents a new result that to our knowledge has not previously appeared in the literature (although we note that the result is similar conceptually, but not in detail, to the work of Raynal *et al.*[57]), and provides a unique means for producing and observing confined flow mixing in microfluidic applications. In this context, the CFM can be considered as a microfluidic analog of the blinking vortex or periodic cavity flow configurations and could be useful in a number of applications involving material study in microfluidic devices.[23,57–59]

In the star-cell geometry, a throughput channel flow is combined with an oscillatory cross flow in order to utilize the CFM mixing mechanism in a continuous mixing operation. This is a perfectly reasonable path to follow and is prevalent in the literature. For example, the eccentric helical annular mixer is a 3D throughput application of the mixing mechanism that generated in a 2D journal bearing flow.[14] In general, all the signatures of chaotic flow present in the CFM are also present in the star-cell, that is, stretching and folding of material lines leading to particle dispersion, positive stretching exponents, and a high degree of mixing.

Two cases were studied for the star-cell, variable throughput rate at a fixed Strouhal number, and fixed throughput rate with variable Strouhal number. Although it might be argued that the latter is the more natural way in which to study the system, there is good reason for studying the former. For purely oscillatory flow in both the CFM and star-cell, a peak degree of mixing was achieved in the system at about St=1.28. Thus, it might be reasoned *a priori* that the

best conditions for continuous mixing in the star-cell would be obtained by using a relatively low throughput rate, at the optimal oscillatory value of St. However, this was found not to be true. At a fixed value of St=1.28, the output stream suffered from segregation effects at low throughput rates, while the high output rates suffered from islands. Thus, based on the particle plots it was reasoned that an intermediate rate gave the best degree of mixing, and this proved true in the degree of mixing calculations.

The fixed throughput, variable St case was used to characterize the degree of mixing for the star-cell. It was found that under these conditions, the degree of mixing increases with Strouhal number until a maximum is reached, followed by plateau regime in which the value of D_m is commensurate with the maximum and changes only very weakly with St. The best mixing was obtained in the star-cell for U=0.16, where the maximum is D_m=0.91 at St=1.28, with a plateau value on the order of $D_m \approx 0.9$ for St$\geq$1.28. The max/plateau level for the degree of mixing appears to be roughly bounded at the high end by the value of D_m obtained in oscillatory flow, and is a slightly decreasing function of the dimensionless flow rate, U. In the plateau regime good mixing is maintained at Strouhal numbers much higher than the optimal oscillatory flow value, indicating that under some conditions there is a synergistic interplay between the throughput and oscillatory flow.

It was observed in the calculations that at the higher throughput rate U=0.32, the ultimate mixing level was below that achieved for U=0.16, and it took a higher Strouhal number to reach the max/plateau region. A number of ideas related to residence time were looked at to explain this behavior. Tracking of individual Lagrangian particles was used to show that under throughput conditions, the particles have a distribution of residence times, in which some particles undergo multiple orbits in the chaotic mixing regime, while others pass through almost immediately. The oscillatory region, therefore, acts in some sense as a temporary "trap" for the particles, where they are mixed for a certain amount of cycles before being convected downstream. Based on this, it seems plausible that the general decrease in the maximum degree of mixing with increasing throughput rate may be traceable in part to a broadening of the RTD with increasing flow rate. Another factor that seems to be important is the average residence time of the particles in the mixing region. It was observed that at constant Strouhal number, the particle holdup in the center mixing region dramatically decreases as the throughput rate increases and that the decreasing holdup is linked with a decrease in degree of mixing, e.g., as occurs when the flow rate is increased from U=0.16 to 0.32 at St =1.28. Since the holdup increases with increasing Strouhal number at constant flow rate, this idea is consistent with the observation that the Strouhal number required to achieve the max/plateau level increases as U increases.

Oscillatory boundary conditions have also been used in other mixing studies, and it is important to understand the relation between various works. A common element we have found is that the TW mechanism is also present in other types of pressure-driven oscillatory flows, but that it occurs in a slightly different manner. For example, we looked for
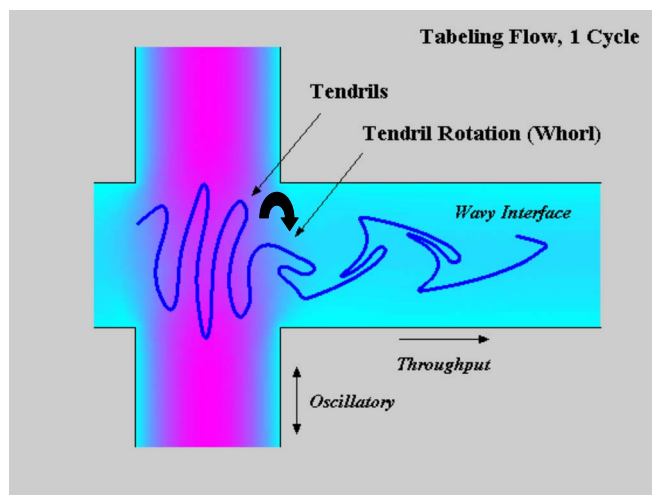

FIG. 21. (Color online) Illustration of the tendril-whorl flow mechanism in the oscillatory flow defined by Tabeling *et al.* (Refs. 46 and 47) and Mezic *et al.* (Ref. 49) for St=1.28 and R_v=0.125.

the TW mechanism in the flow discussed by Tabeling[46,47] (see Fig. 21), where the flow is sinusoidal in the vertical direction and steady in the lateral direction. The deformation of a material line (initially centered upstream) passing through the oscillatory section is shown in Fig. 21 for the case of St=1.28 and a ratio of lateral to oscillatory velocity of R_v=0.125. The TW mechanism is clearly present as tendrils are formed in the line as it passes through the middle of the oscillatory section, and then each tendril alternately rotates either $\pm120°$ (for these particular parameters) as it passes to the downstream flow. For a single oscillatory channel, this produces a wavy interface. However, when multiple oscillatory units are used and the TW mechanism is repeated, the flow becomes chaotic, as has been shown by Mezic *et al.*[49] This, more than anything else, can help us to understand the similarities and differences between the two cases. The kinematics produced by the two intersecting oscillating streams in the CFM/star-cell type mixer act to create what might be termed a continuous TW flow, whereas the flows based on a single oscillating stream produce a discrete amount of stretching and rotation with each pass through an oscillatory section. Thus, in terms of net stretching and rotation, there is an equivalence between a fluid spending multiple cycles in the mixing region of the CFM type flow, and passing through multiple oscillatory sections in the latter.

A number of items might be the object of future work. It does not appear that brute force extension of the calculations up to much higher Strouhal numbers is warranted. The present calculations up to a value of St=3.2 were more than adequate to demonstrate the basic physics of the transition to chaos and trends that are seen with increasing throughput flow. These calculations show that to a large extent, the best mixing conditions seem to revolve around the optimal oscillatory value of St=1.28. Therefore, a more detailed sweep of the parameter space in this region might be in order, as these might reveal some local maxima. An exception to this might be the mixing of immiscible components in the system. Under those conditions, the greater draw ratios achieved using

higher Strouhal numbers might be beneficial to interface breakup.

Another idea that warrants investigation in future work is the use of mixed frequency or multifrequency waveforms more complex than the simple sinusoidal oscillations employed here. This approach is suggested by the synergy that is sometimes observed between the throughput and oscillatory flow for continuous mixing in the star-cell, and may be especially helpful for the case of confined mixing in the CFM, which is limited at high St by the growth of islands. If such means can be used to increase the degree of mixing in the CFM, it might also provide improvement in the star-cell as well. A final idea that is interesting from a theoretical viewpoint is to use the third direction normal to the spatio-temporal oscillations in the 2D plane as the throughput direction for continuous mixing, i.e., a 3D flow configuration. While this brings us slightly out of the simple planar flows most often seen in microfluidics, it has been shown to be effective in the past. For example, this was the means for extending confined mixing in the journal bearing flow to continuous mixing in the eccentric helical annular mixer.[14]

SUMMARY AND CONCLUSIONS

The kinematics of oscillatory flow in intersecting channels has been studied numerically as a means for generating chaotic mixing in microfluidic devices for confined mixing in a cross-flow mixer, and continuous mixing in the star-cell geometry. Chaotic flow is generated in both configurations by a tendril-whorl flow mechanism, which is created when sinusoidally driven, out-of-phase fluid streams cross each other in the flow domain, consistent with the principle of crossing spatio-temporal streamlines as a necessary condition for generating chaos. The study of purely oscillatory motion allowed identification of boundary condition regimes that are viable for producing chaotic mixing and represents the maximum possible effective mixing that can be obtained from a given flow configuration. Calculations show that the CFM provides a simple and convenient means to generate chaotic flow in microfluidic devices under confined conditions, and has a peak degree of mixing on the order of 90%. In the star-cell configuration, the effect of combining a fixed throughput flow with oscillatory motion as a means for generating continuous mixing was examined, and it was shown that a degree of mixing in the 80%–90% range can be achieved. The max/plateau level for the degree of mixing
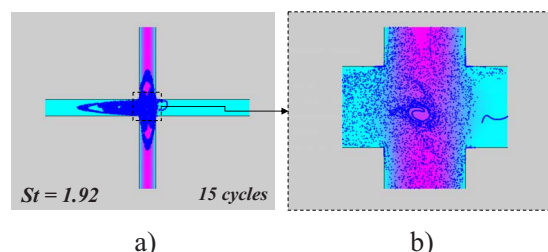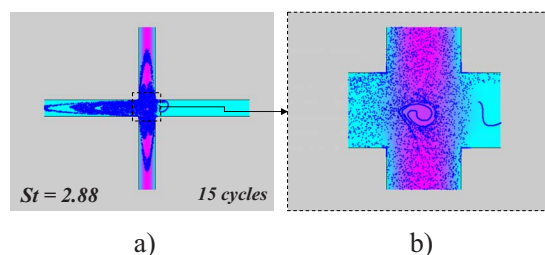

FIG. 23. (Color online) Stretching of a material line in the CFM as a function of Strouhal number after 15 cycles for St=2.88. (a) Wide angle view equivalent to that in Fig. 22. The expansion of the chaotic region and the growth of the islands at the tips of the chaotic region (relative to Fig. 22) are evident. (b) Detail showing the emergence of island in the center of the flow.

appears to be roughly bounded at the high end by the value of D_m obtained in oscillatory flow, and is a slightly decreasing function of the dimensionless flow rate, U. A maximum D_m on the order of 90% was obtained for $U=0.16$ and St ≥ 1.28. The study suggests a number of ideas that might be pursued in future work, including multifrequency oscillations, 3D flow, as well as experimental inquiry.

APPENDIX: PARTICLE DISPERSION IN THE CROSS-FLOW MIXER AT HIGHER STROUHAL NUMBERS

In Figs. 2(a)–2(d), the stretching of a material line in the CFM as a function of Strouhal number is used to show the transition to chaotic behavior as the Strouhal number increases. Figures 22 and 23 depict the particle dispersion after 15 cycles at higher Strouhal numbers, St=1.92 and 2.88, respectively. The figures show that the chaotic region continues to expand along the length of the channel as St increases. However, the overall growth in size of the chaotic region is accompanied by an increase in the size of existing islands and the growth of new ones. In particular, the eyelet islands near the tips of the chaotic region [cf. Fig. 2(d)] are appreciably larger in Figs. 22(a) and 23(a). In addition, a new island emerges at the center of the geometry that grows appreciably in size as indicated in part (b) of the figures. The growth of the center island is the main reason for the decline in the degree of mixing for St > 1.28.

[1]H. A. Stone, A. D. Stroock, and A. Ajdari, "Engineering flows in small devices: Microfluidics toward a lab-on-a-chip," Annu. Rev. Fluid Mech. **36**, 381 (2004).

[2]J. M. Ottino and S. Wiggins, "Introduction: Mixing in microfluidics," Philos. Trans. R. Soc. London, Ser. A **362**, 923 (2004).

[3]J. M. Ottino, *The Kinematics of Mixing: Stretching, Chaos, and Transport* (Cambridge University Press, Cambridge, UK, 1989).

[4]J. M. Ottino, "The mixing of fluids," Sci. Am. **260**, 56 (1989).

[5]S. Wiggins and J. M. Ottino, "Foundations of chaotic mixing," Philos. Trans. R. Soc. London, Ser. A **362**, 937 (2004).

[6]J. M. Ottino, P. DeRoussel, S. Hansen, and D. V. Khakhar, "Mixing and dispersion of viscous liquids and powdered solids," Adv. Chem. Eng. **25**, 105 (2000).

[7]J. M. Ottino, S. C. Jana, and V. S. Chakravarthy, "From Reynolds stretching and folding to mixing studies using horseshoe maps," Phys. Fluids **6**, 685 (1994).

[8]C. W. Leong and J. M. Ottino, "Experiments on mixing due to chaotic advection in a cavity," J. Fluid Mech. **209**, 463 (1989).

[9]M. F. Doherty and J. M. Ottino, "Chaos in deterministic systems—Strange attractors, turbulence, and applications in chemical engineering," Chem. Eng. Sci. **43**, 139 (1988).

FIG. 22. (Color online) Stretching of a material line in the CFM as a function of Strouhal number after 15 cycles for St=1.92. (a) Wide angle view. (b) Detail showing the emergence of an island in the center of the flow.

[10] J. G. Franjione and J. M. Ottino, "Stretching in duct flows," Phys. Fluids A **3**, 2819 (1991).

[11] J. M. Ottino and S. Wiggins, "Designing optimal micromixers," Science **305**, 485 (2004).

[12] D. V. Khakhar, H. Rising, and J. M. Ottino, "Analysis of chaotic mixing in two model systems," J. Fluid Mech. **172**, 419 (1986).

[13] S. C. Jana, M. Tjahjadi, and J. M. Ottino, "Chaotic mixing of viscous fluids by periodic changes in geometry—Baffled cavity flow," AIChE J. **40**, 1769 (1994).

[14] H. A. Kusch and J. M. Ottino, "Experiments on mixing in continuous chaotic flows," J. Fluid Mech. **236**, 319 (1992).

[15] F. J. Muzzio, P. D. Swanson, and J. M. Ottino, "The statistics of stretching and stirring in chaotic flows," Phys. Fluids A **3**, 822 (1991).

[16] P. D. Swanson and J. M. Ottino, "A comparative computational and experimental study of chaotic mixing of viscous fluids," J. Fluid Mech. **213**, 227 (1990).

[17] W. L. Chien, H. Rising, and J. M. Ottino, "Laminar mixing and chaotic mixing in several cavity flows," J. Fluid Mech. **170**, 355 (1986).

[18] H. Aref, "The development of chaotic advection," Phys. Fluids **14**, 1315 (2002).

[19] H. Aref, "Chaotic advection in perspective," Chaos, Solitons Fractals **4**, 745 (1994).

[20] H. Aref, "Chaotic advection of fluid particles," Philos. Trans. R. Soc. London, Ser. A **333**, 273 (1990).

[21] H. Aref, S. W. Jones, S. Mofina, and I. Zawadzki, "Vortices, kinematics and chaos," Physica D **37**, 423 (1989).

[22] H. Aref, "Stirring by chaotic advection," J. Fluid Mech. **143**, 1 (1984).

[23] M. A. Stremler, F. R. Haselton, and H. Aref, "Designing for chaos: Applications of chaotic advection at the microscale," Philos. Trans. R. Soc. London, Ser. A **362**, 1019 (2004).

[24] E. Ott, *Chaos in Dynamical Systems* (Cambridge University Press, Cambridge, UK, 1993).

[25] P. DeRoussel, D. V. Khakhar, and J. M. Ottino, "Mixing of viscous immiscible liquids. Part 1: Computational models for strong-weak and continuous flow systems," Chem. Eng. Sci. **56**, 5511 (2001).

[26] P. DeRoussel, D. V. Khakhar, and J. M. Ottino, "Mixing of viscous immiscible liquids. Part 2: Overemulsification—Interpretation and use," Chem. Eng. Sci. **56**, 5531 (2001).

[27] J. M. Ottino, "Unity and diversity in mixing—Stretching, diffusion, breakup, and aggregation in chaotic flows," Phys. Fluids A **3**, 1417 (1991).

[28] A. D. Stroock, S. K. Dertinger, G. M. Whitesides, and A. Ajdari, "Patterning flows using grooved surfaces," Anal. Chem. **74**, 5306 (2002).

[29] A. D. Stroock, S. K. W. Dertinger, A. Ajdari, I. Mezic, H. A. Stone, and G. M. Whitesides, "Chaotic mixer for microchannels," Science **295**, 647 (2002).

[30] H. Z. Wang, P. Iovenitti, E. Harvey, and S. Masood, "Numerical investigation of mixing in microchannels with patterned grooves," J. Micromech. Microeng. **13**, 801 (2003).

[31] J. T. Yang, K. J. Huang, and Y. C. Lin, "Geometric effects on fluid mixing in passive grooved micromixers," Lab Chip **5**, 1140 (2005).

[32] Y. Z. Liu, B. J. Kim, and H. J. Sung, "Two-fluid mixing in a microchannel," Int. J. Heat Fluid Flow **25**, 986 (2004).

[33] H. Song, M. Bringer, J. Tice, C. Gerdts, and R. Ismagilov, "Experimental test of scaling of mixing by chaotic advection in droplets moving through microfluidic channels," Appl. Phys. Lett. **83**, 4664 (2003).

[34] R. H. Liu, M. A. Stremler, K. V. Sharp, M. G. Olsen, J. G. Santiago, R. J. Adrian, H. Aref, and D. J. Beebe, "Passive mixing in a three-dimensional serpentine microchannel," J. Microelectromech. Syst. **9**, 190 (2000).

[35] M. Muradoglu and H. A. Stone, "Mixing in a drop moving through a serpentine channel: A computational study," Phys. Fluids **94**, 073305 (2005).

[36] Z. B. Stone and H. A. Stone, "Imaging and quantifying mixing in a model droplet micromixer," Phys. Fluids **17**, 063103 (2005).

[37] V. Hessel, S. Hardt, C. Hofmann, H. Pennemann, and F. Schonfeld, "Micro mixing principles and applications—A review on specific multi-lamination, split-recombine and chaotic approaches," Abstr. Pap. - Am. Chem. Soc. **226**, U42 (2003).

[38] F. Schonfeld, V. Hessel, and C. Hofmann, "An optimised split-and-recombine micro-mixer with uniform 'chaotic' mixing," Lab Chip **4**, 65 (2004).

[39] K. Mae, T. Maki, I. Hasegawa, U. Eto, Y. Mizutani, and N. Honda, "Development of a new micromixer based on split/recombination for mass production and its application to soap free emulsifier," Chem. Eng. J. **101**, 31 (2004).

[40] T. H. Solomon and I. Mezic, "Uniform resonant chaotic mixing in fluid flows," Nature (London) **425**, 376 (2003).

[41] T. H. Solomon, S. Tomas, and J. L. Warner, "Chaotic mixing of immiscible impurities in a two-dimensional flow," Phys. Fluids **10**, 342 (1998).

[42] J. A. Pathak, D. Ross, and K. B. Migler, "Elastic flow instability, curved streamlines and mixing in microfluidic flows," Phys. Fluids **16**, 4028 (2004).

[43] A. Groisman and V. Steinberg, "Efficient mixing at low Reynolds numbers using polymer additives," Nature (London) **410**, 905 (2001).

[44] S. R. Deshmukh and D. G. Vlachos, "Novel micromixers driven by flow instabilities: Application to post-reactors," AIChE J. **51**, 3193 (2005).

[45] R. A. Truesdell, P. V. Vorobieff, L. A. Sklar, and A. A. Mammoli, "Mixing of a continuous flow of two fluids due to unsteady flow," Phys. Rev. E **67**, 066304 (2003).

[46] F. Okkels and P. Tabeling, "Spatiotemporal resonances in mixing of open viscous fluids," Phys. Rev. Lett. **92**, 038301 (2004).

[47] P. Tabeling, M. Chabert, A. Dodge, C. Jullien, and F. Okkels, "Chaotic mixing in cross-channel micromixers," Philos. Trans. R. Soc. London, Ser. A **362**, 987 (2004).

[48] X. Z. Niu and Y. K. Lee, "Efficient spatial-temporal chaotic mixing in microchannels," J. Micromech. Microeng. **13**, 454 (2003).

[49] F. Bottausci, I. Mezic, C. D. Meinhart, and C. Cardonne, "Mixing in the shear superposition micromixer: Three-dimensional analysis," Philos. Trans. R. Soc. London, Ser. A **362**, 1001 (2004).

[50] R. A. Truesdell, J. W. Bartsch, T. Buranda, L. A. Sklar, and A. A. Mammoli, "Direct measurement of mixing quality in a pulsatile flow micromixer," Exp. Fluids **39**, 819 (2005).

[51] I. Glasgow, J. Batton, and N. Aubry, "Electroosmotic mixing in microchannels," Lab Chip **4**, 558 (2004).

[52] Identification of a commercial product is made only to facilitate reproducibility and to adequately describe procedure. In no case does it imply endorsement by the National Institute of Standards and Technology (NIST) or that it is necessarily the best product for the procedure.

[53] *COMSOL MP User's Guide* (COMSOL AB, Burlington, MA, 2006).

[54] *MATLAB User's Guide* (Mathworks, Natick, MA, 2004).

[55] While ergodicity may be quantitatively proven, we use it here in the qualitative sense that particles tend to disperse homogeneously within a KAM surface in the flow domain, independent of initial configuration, and that the resulting dispersion patterns are indistinguishable from each another.

[56] T. G. Kang and T. H. Kwon, "Colored particle tracking method for mixing analysis of chaotic micromixers," J. Micromech. Microeng. **14**, 891 (2004).

[57] F. Raynal, F. Plaza, A. Beuf, P. Carriere, E. Souteyrand, J.-R. Martin, J.-P. Cloarec, and M. Cabrera, "Study of chaotic mixing system for DNA chip hybridization chambers," Phys. Fluids **16**, L63 (2004).

[58] K. Jo, E. Dimalanta, Y. L. Chen, R. Runnheim, H. B. Ma, M. D. Graham, J. J. de Pablo, S. N. Coppersmith, and D. C. Schwartz, "Fluid arrays: Shear induced migration of single DNA molecules in confined environments," Biophys. J. **88**, 658A (2005).

[59] N. Y. Lee, M. Yamada, and M. Seki, "Development of a passive micromixer based on repeated fluid twisting and flattening, and its application to DNA purification," Anal. Bioanal. Chem. **383**, 776 (2005).